Synthesis Of Nitrogen-Doped Graphene Films For Lithium Battery Application

Arava Leela Mohana Reddy,[†,*] Anchal Srivastava,[†] Sanketh R. Gowda,[‡] Hemtej Gullapalli,[†] Madan Dubey,[§] and Pulickel M. Ajayan[†,*]

[†]Department of Mechanical Engineering and Materials Science, Rice University, Houston, Texas 77005, United States, [‡]Department of Chemical and Biomolecular Engineering, Rice University, Houston, Texas 77005, United States, and [§]U.S. Army Research Laboratory, 2800 Powder Mill Road, Adelphi, Maryland 20783, United States

ABSTRACT We demonstrate a controlled growth of nitrogen-doped graphene layers by liquid precursor based chemical vapor deposition (CVD) technique. Nitrogen-doped graphene was grown directly on Cu current collectors and studied for its reversible Li-ion intercalation properties. Reversible discharge capacity of N-doped graphene is almost double compared to pristine graphene due to the large number of surface defects induced due to N-doping. All the graphene films were characterized by Raman spectroscopy, transmission electron microscopy, and X-ray photoemission spectroscopy. Direct growth of active electrode material on current collector substrates makes this a feasible and efficient process for integration into current battery manufacture technology.

KEYWORDS: nitrogen-doped graphene · surface defects · chemical vapor deposition · Li-battery · anode · cyclic performance

Carbon-based rechargeable batteries have gained extensive attention, particularly after the commercialization of the Li-ion battery from Sony laboratories,[1] wherein metallic lithium is replaced by a carbon host structure that can reversibly absorb and release lithium ions at low electrochemical potentials. There have been several efforts to increase the energy density and specific capacity of these cells by using many types of industrially available and heat-treated carbons.[2−5] Chemical dopants in carbon materials such as phosphorus,[6−8] boron,[9−11] and boron−nitrogen[12,13] showed a substantial increase in specific capacity relative to pure carbon structures. Several research attempts focused on developing carbon nanotubes based energy storage/conversion devices are still under development stage.[14−20] All the graphitic forms of carbon including zero-dimensional fullerenes, one-dimensional carbon nanotubes, and three-dimensional graphite are essentially derived from the two-dimensional, single atomic layer, graphene structure.[21] The two-dimensional graphene has been considered as a potential electrode material for Li-ion battery applications, primarily due to its superior electrical conductivity, high surface area, and a broad electrochemical window.[22−25] Recent reports have shown it to be a promising electrode material for electrochemical devices such as Li-ion batteries, supercapacitors, and so on. Chemical reduction of graphite oxide resulting in high surface area (few layer) reduced GO has been the predominant method of synthesis of graphene electrodes for Li battery applications. After the synthesis of reduced GO powder an additional step of coating this electrode material on to the current collector is required for thin film battery fabrication. The weak adherence between the electrode and current collector results in a poor electron transport and loss of electrical contact on extended cycling. Hence, there is a need for direct fabrication of graphene electrode materials on current collector substrates. The atomically thin nature and high surface area of the graphene electrodes grown directly on current collector substrates make them an excellent choice for electrodes in Li-ion high power thin film batteries.

Further, nitrogen- and boron-doped graphene structures have attracted considerable interest in the field of electronics.[26−28] Like other doped carbon forms, nitrogen-doped graphene is expected to have enhanced Li-battery properties.[13] Reports on the synthesis of nitrogen-doped graphene are very scarce, and hence, developing a simple method to synthesize N-doped graphene is noteworthy. Recently, we were successful in synthesizing a new form of 2D atomic film consisting of hybridized h-BN and C by a chemical vapor deposition technique.[29] Hence, it is of fundamental interest to investigate how N-doping in graphene affects Li interaction properties when compared to pristine graphene. With

*Address correspondence to ajayan@rice.edu, leela@rice.edu.

Received for review August 5, 2010 and accepted October 03, 2010.

Published online October 8, 2010. 10.1021/nn101926g

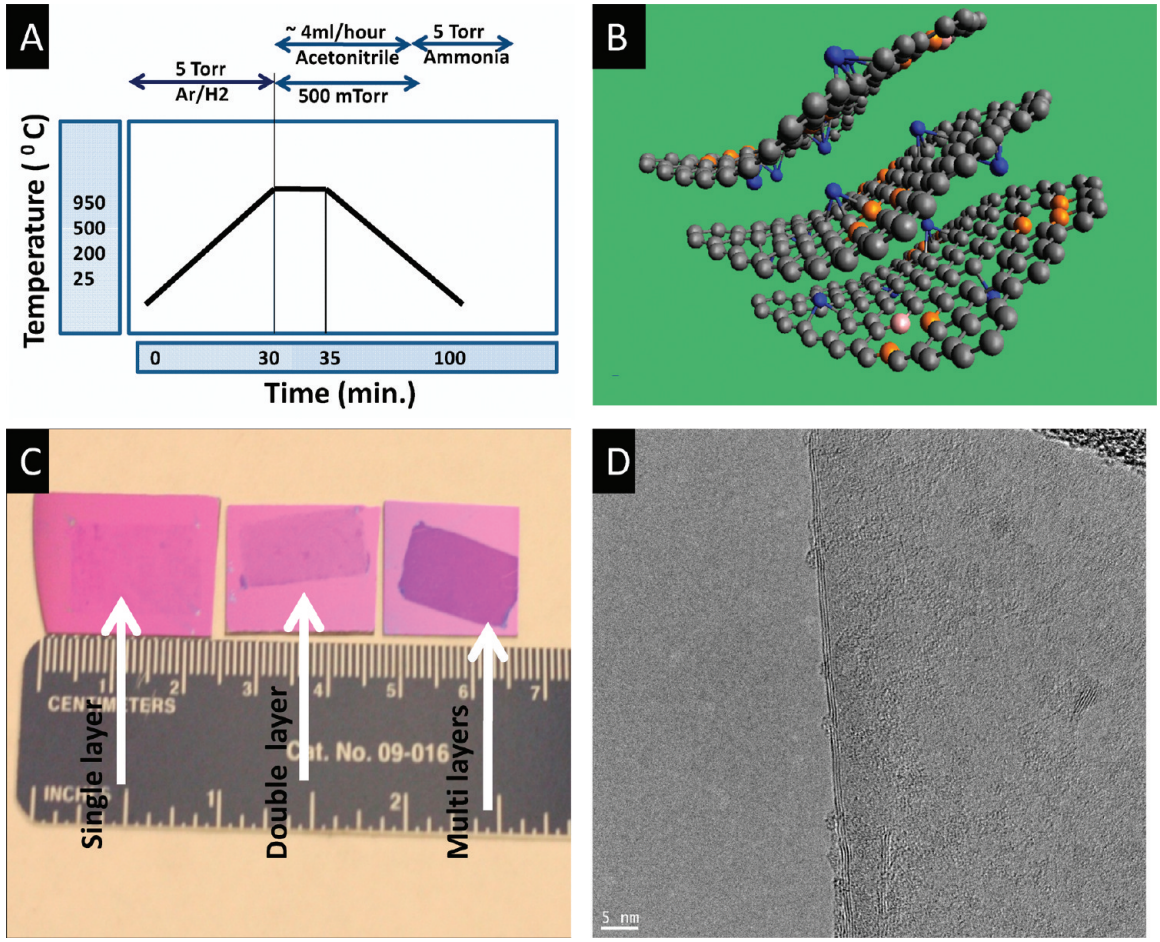

Figure 1. (A) Schematic representation of optimized experimental parameters (temperature profile, liquid and gas flow rates, and system pressure) for the growth of N-doped graphene films on Cu foil. (B) Schematic representation of the N-doped graphene layer. The gray spheres represent carbon atoms, blue spheres represent graphitic N atoms, orange spheres represent pyridinic N atoms, and pink spheres represent pyrrolic N atoms. (C) Optical images of mono-layer, double-layered, and multi-layered N-doped graphene films transferred on Si/SiO_2 substrate. (D) High resolution TEM images of three-layered N-doped graphene.

this motivation, we have synthesized pristine and N-doped graphene materials directly on large copper current collector substrates by liquid phase chemical vapor deposition technique and studied their Li intercalation properties. Continuous, few layer, nitrogen-doped graphene was grown on 25 μm thick Cu foil by chemical vapor deposition technique using acetonitrile as the liquid precursor.

RESULTS AND DISCUSSION

Figure 1A shows the schematic representation of optimized experimental parameters (temperature profile, precursor and ammonia gas flow rates, and system pressure) for the growth of N-doped graphene. The number of graphene layers was controlled by adjusting the time of acetonitrile flow while keeping other parameters constant. Figure 1B is the schematic representation of the N-doped graphene. The grey spheres represent carbon atoms, blue spheres represent graphitic N atoms, orange spheres represent pyridinic N atoms and pink spheres represent pyrrolic N atoms. Figure 1C shows the optical images of mono-layer, double-layered, and multi-layered N-doped graphene on Si/SiO_2 substrates. The optical image clearly indicates that the film looks darker with increase in number of graphene layers. Figure 1D shows high resolution TEM images of three-layered N-doped graphene. A further increase of deposition time resulted in deposition of amorphous carbon along with crystalline graphene.

Figure 2A shows the Raman spectra of few layered N-doped graphene samples. The most characteristic feature of graphene is the presence of 2D band in the Raman spectra. As seen from Figure 2A, N-doped graphene showed a sharp 2D peak at 2697 cm^{-1} and tangential mode G-band at 1587 cm^{-1}. The high intensity of the D-band (around 1356 cm^{-1}) in the N-doped graphene films clearly indicates the presence of defects in the graphene layer; these defects are usually generated during nitrogen doping. The Raman spectra of pristine graphene films grown using hexane vapors (shown in Supporting Information, Figure S1) clearly shows that the intensity of D-band is much less compared to N-doped graphene.

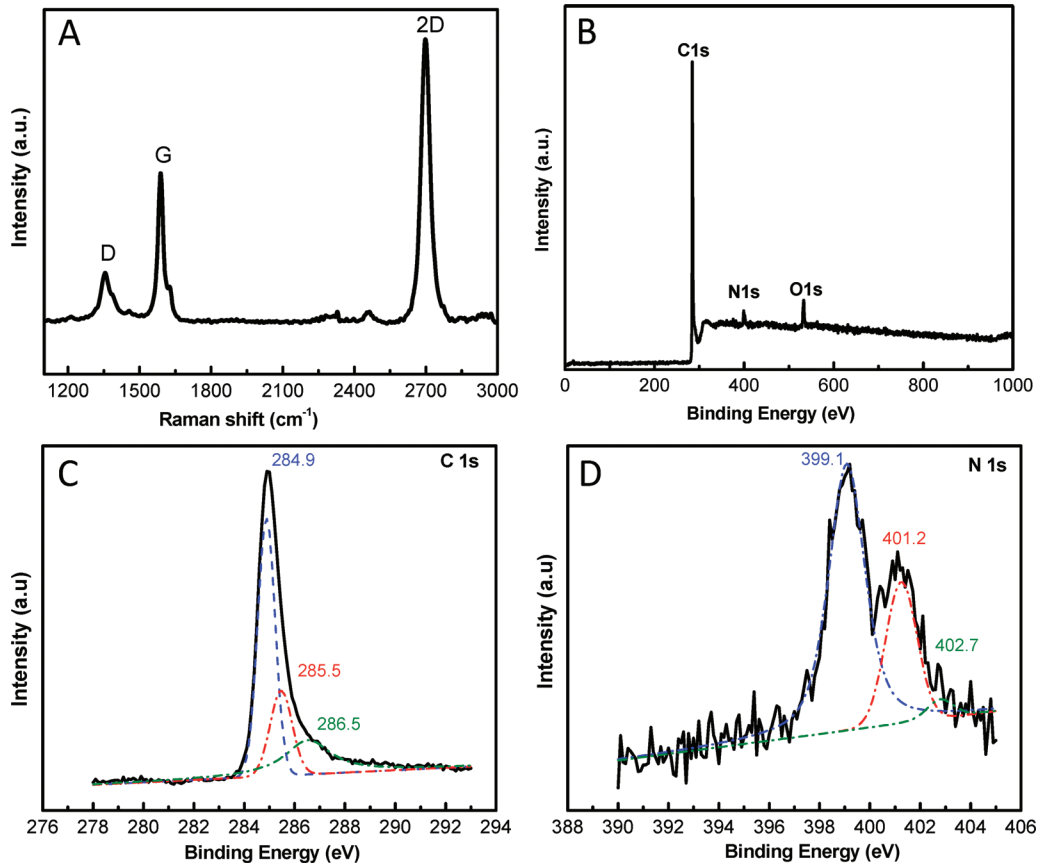

Figure 2. (A) Raman spectra of the N-doped graphene having one to two layers in it. (B) XPS spectra of the N-doped graphene. (C) XPS C1s spectrum, which can be split in to three Lorentzian peaks at 284.9, 285.5, and 286.5 eV, and (D) XPS N1s spectrum of the N-doped graphene. The N1s peak can be split into three Lorentzian peaks at 399.1, 401.2, and 402.7 eV.

To confirm N-doping of graphene, X-ray photoemission spectroscopy (XPS) studies were carried out. The survey scan spectrum from XPS analysis showed the presence of the principal C1s, O1s, and N1s core levels, with no evidence of impurities (Figure 2B), and an atomic percentage of doped nitrogen to be about 9%. The spectrum was corrected for any background signals using the Shirley algorithm[30] prior to curve resolution. The C1s core level peak can be resolved into three components centered at ~284.9, 285.5, and 286.5 eV represents sp^2C-sp^2C, N-sp^2C and N-sp^3C bonds, respectively (Figure 2C). Similarly, the N1s peak can also be resolved into three components centered at 399.1, 401.2, and 402.7 eV representing pyridinic, pyrrolic, and graphitic type of N atoms doped in the graphene structure (Figure 2D). Similarly, XPS spectra of pristine graphene, shown in Supporting Information, Figure S2, clearly shows the presence of C1s and O1s core levels with no trace of impurities.

Figure 3 delineates the electrochemical properties of the N-doped graphene films. Figure 3A shows the cyclic voltammogram of the N-doped graphene electrode conducted at a scan rate of 0.1 mV s^{-1} in 1 M solution of $LiPF_6$ in 1:1 (v/v) mixture of ethylene carbonate (EC) and dimethyl carbonate (DMC) as an electrolyte against Li as counter and reference electrode. The CV measurement of the N-doped graphene electrodes showed that lithium could reversibly intercalate and deintercalate into graphene layers. The lithium insertion potential is quite low, which is very close to 0 V *versus* the Li^+/Li reference electrode, whereas the potential for lithium deintercalation is in the range of 0.2−0.3 V. Figure 3B shows the voltage *versus* specific capacity plots conducted at 5 μA/cm^2 between 3.2 and 0.02 V *versus* Li/Li^+. The first discharge curve shows a plateau at about 0.7 V. This discharge plateau can be attributed to the formation of an SEI film (solid electrolyte interface) on the surface of the graphene, which is associated with electrolyte decomposition and the formation of lithium organic compounds.[31,32] In the subsequent cycles, this discharge plateau disappeared. A reversible capacity of 0.05 mAh/cm^2 was obtained in the subsequent cycles. The first cycle showed a discharge capacity of around 0.25 mAh/cm^2 and loss in capacity was observed in the second cycle (~0.08 mAh/cm^2) due to the SEI formation, very commonly observed in carbon-based electrodes. Voltage *versus* time profiles for the first 10 cycles are shown in Supporting Information, Figure S3.

Finally, a comparison study of the cyclic characteristics of the N-doped graphene and pristine graphene was conducted. Both N-doped graphene and pristine

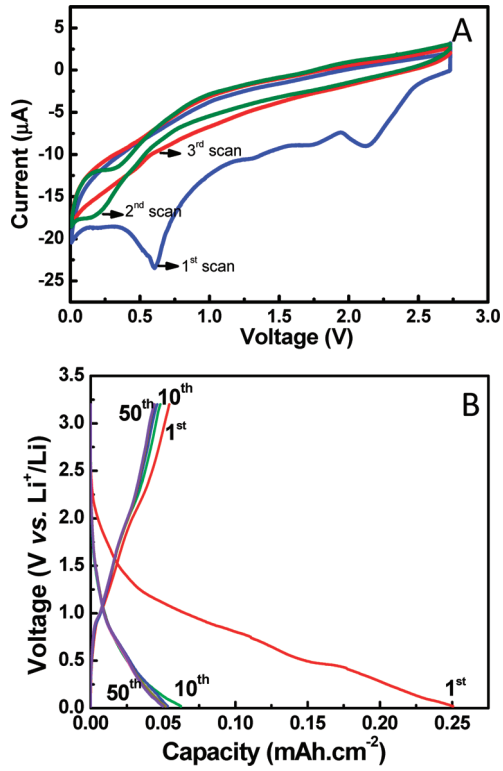

Figure 3. Electrochemical performance of N-doped graphene films grown on Cu foil. (A) Cyclic voltammograms of N-doped graphene electrode in 1 M solution of $LiPF_6$ in 1:1 (v/v) mixture of ethylene carbonate (EC) and dimethyl carbonate (DMC) as the electrolyte with Li as counter and reference electrode (scan rate: 0.1 mV s^{-1}); (B) Charge−discharge voltage profiles for the N-doped graphene electrode cycled at a rate of 5 μA/cm^2 between 3.2 and 0.02 V *vs* Li/Li^+.

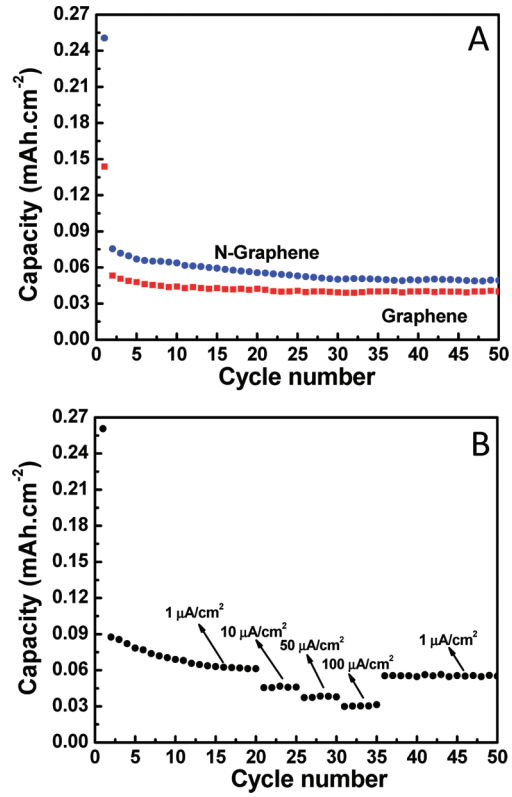

Figure 4. Electrochemical performance of graphene films grown on Cu foil, galvanostatically cycled in Li half cells. (A) Variation in discharge capacity *vs* cycle number for the pristine graphene and N-doped graphene cycled at a rate of 5 μA/cm^2 between 3.2 and 0.02 V *vs* Li/Li^+ in 1 M solution of $LiPF_6$ in 1:1 (v/v) mixture of ethylene carbonate (EC) and dimethyl carbonate (DMC) as the electrolyte. (B) Rate capability studies of N-doped graphene films: Discharge capacity *vs* cycle number at various current rates (1, 10, 50, and 100 μA/cm^2).

graphene (Supporting Information, Figure S4) were cycled at 5 μA/cm^2 between 3.2 and 0.02 V *versus* Li/Li^+ for 50 cycles. Figure 4A shows the specific capacity *versus* cycle number plots for the graphene and the N-doped graphene. Pristine and N-doped graphene shows reversible discharge capacities of 0.05 and 0.03 mAh/cm^2, respectively. The increase in the reversible discharge capacity of N-doped graphene over pristine graphene can be attributed to the topological defects induced in the N-doped graphene electrode. First, a large number of surface defects are induced onto the graphene films by N-doping, which leads to the formation of a disordered carbon structure that further enhances Li intercalation properties.[33] As observed in the XPS data, the N-doped graphene also has a high percentage of pyridinic N atoms present in it. The pyridinic N atoms could also be involved in the improvement of reversible capacity of the N-doped graphene electrode compared to the pristine graphene electrode.[34] Electrical contact between the electrode and current collector plays an important role in the power capability of the Li-ion battery. Good electrical contact between the electrode and current collector was realized by the direct growth of graphene on copper foil. Figure 4B shows the detailed high rate cycling results for the N-doped graphene electrode. Galvanostatic charge/discharge experiments were conducted at various currents to investigate the rate capability of the electrode material. Stable nominal capacity was attained at a current rate of 1 μA/cm^2 corresponding to a C-rate of C/60. Subsequent cycles were cycled at higher current rates, as shown in Figure 4B. Even at very high current rates of operation, such as 100 μA/cm^2, excellent capacity retention of 60% of the nominal capacity was observed. On returning to the low current rate of 1 μA/cm^2, the nominal capacity (~0.06 mAh/cm^2) is comparable with previously reported values of carbon-based thin film electrodes.[35] The results of high rate electrochemical studies prove that the N-doped graphene electrode could be used as an excellent high rate electrode. The direct contact between the N-doped graphene electrode and the current collector leads to reduced electronic resistance, hence, resulting in a high electrode rate capability.

CONCLUSIONS

Our results here throw new insights into the Li intercalation into N-doped carbon nanaostructures. We have demonstrated enhanced Li-ion intercalation in pristine

graphene electrode by inducing surface defects and introducing pyridinic N atoms into the graphene structure. These results agree well with previous theoretical predictions of the improved Li-ion intercalation for pyridinic N atom doped carbon nanotubes. Reversible discharge capacity of N-doped graphene is almost double compared to pristine graphene due to the large number of surface defects induced due to N-doping. Our unique liquid precursor based synthesis also ensures the fabrication of N-doped graphene films with a high percentage of pyridinic N atoms responsible for the enhanced Li-ion intercalation properties. Direct growth on current collector substrates makes this a feasible process to integrate into current battery manufacture technology. The high performance N-doped graphene electrodes could find vast application in flexible thin film batteries.

EXPERIMENTAL SECTION

One to few layers of both pristine graphene and N-doped graphene films on Cu substrate were synthesized by chemical vapor deposition technique using hexane and acetonitrile precursors, respectively. Initially, Cu foil was loaded in Quartz tube of a CVD furnace and evacuated to a base pressure of 10^{-2} Torr. The furnace was then heated to 950 °C, while flowing Ar/H_2 and maintaining a pressure of 5 Torr. Once the desired temperature is reached, Ar/H_2 gas was stopped and acetonitrile vapors were passed while maintaining the tube pressure at 500 mTorr. The duration of vapors correlates to the number of desired graphene layers. A total of 3−15 min of vapor flow would typically result in 1 or few layer graphene. The furnace is then cooled to room temperature with a flow of ammonia gas. As-grown nitrogen-doped graphene films on the Cu foil were used for all electrochemical studies. For the synthesis of pristine graphene films, all the above parameters were kept constant except liquid precursor and cooling gas. Hexane was used as the liquid precursor while the cooling gas was Ar/H_2. For structural and morphological characterization, the graphene films were transferred on to other substrates. The graphene film on the copper foil was coated with poly methyl methacrylate (PMMA) and then floated in dilute HNO_3. After Cu was dissolved, the PMMA graphene film was lifted from the solution on to other substrates such as SiO_2/Si or ITO. The PMMA was later dissolved with acetone and washed off with iso-propanal alcohol (IPA).

Morphological and elemental analysis of N-doped graphene films were carried out using a transmission electron microscope (JEOL 2010 at 100 kV) by transferring graphene and N-doped graphene samples on to copper grids. X-ray photoemission spectroscopy (XPS) studies were carried out with a spectrophotometer (PHI Quantera SXM) using the monochromatic Al K_α radiation (1486.6 eV). Vibrational properties of N-doped graphene samples were analyzed using Renishaw Raman spectrometer by exciting a 514.5 nm Ar-ion laser. Electrochemical measurements were performed in a Swagelok-type cell using ARBIN BT 2010 Battery Analyzer. For the half cell measurements, an electrochemical test cell was assembled in argon-filled glovebox using the graphene/N-doped graphene as working electrode, lithium metal foil as the counter/reference electrode and 1 M solution of $LiPF_6$ in 1:1 (v/v) mixture of ethylene carbonate (EC) and dimethyl carbonate (DMC).

Acknowledgment. We thank the Army Research Office for funding support.

Supporting Information Available: Raman spectra and XPS spectra of the pristine graphene, voltage *versus* time profiles of N-doped graphene, and voltage *versus* capacity profiles of pristine graphene. This material is available free of charge *via* the Internet at http://pubs.acs.org.

REFERENCES AND NOTES

1. Nagaura, T.; Tozawa, K. Lithium ion rechargeable battery. *Prog. Batteries Solar Cells* **1990**, *9*, 209.
2. Dahn, J.; Sleigh, A.; Shi, H.; Reimers, J.; Zhong, Q.; Way, B. Dependence of the electrochemical intercalation of lithium in carbons on the crystal structure of the carbon. *Electrochim. Acta* **1993**, *38*, 1179–1191.
3. Yoshino, A.; Sanechika, K.; Nakajima, T. U.S. Patent 4668595, 1987.
4. Fong, R.; von Sacken, U.; Dahn, J. R. Studies of lithium intercalation into carbons using nonaqueous electrochemical cells. *J. Electrochem. Soc.* **1990**, *137*, 2009–2013.
5. Dahn, J.; Fong, R.; Spoon, M. Suppression of staging in lithium-intercalated carbon by disorder in the host. *Phys. Rev. B* **1990**, *42*, 6424–6432.
6. Wu, Y.; Fang, S.; Jiang, Y. Carbon anode materials based on melamine resin. *J. Mater. Chem.* **1998**, *8*, 2223–2227.
7. Tran, T. D. Commercial carbonaceous materials as lithium intercalation anodes. *J. Electrochem. Soc.* **1995**, *142*, 3297.
8. Wu, Y. P.; Fang, S.; Jiang, Y.; Holze, R. Effects of doped sulfur on electrochemical performance of carbon anode. *J. Power Sources* **2002**, *108*, 245–249.
9. Way, B. M.; Dahn, J. R. The effect of boron substitution in carbon on the intercalation of lithium in $Li_x(B_zC_{1-z})_6$. *J. Electrochem. Soc.* **1994**, *141*, 907–912.
10. Flandrois, S. Boron-substituted carbons and their intercalation compounds. *J. Phys. Chem. Solids* **1996**, *57*, 741–744.
11. Endo, M. Anode performance of a Li ion battery based on graphitized and B-doped milled mesophase pitch-based carbon fibers. *Carbon* **1999**, *37*, 561–568.
12. Weydanz, W. J.; Way, B. M.; van Buuren, T.; Dahn, J. R. Behavior of nitrogen-substituted carbon ($N_z C_{1-z}$) in $Li/Li(N_zC_{1-z})_6$] cells. *J. Electrochem. Soc.* **1994**, *141*, 900–907.
13. Morita, M.; Hanada, T.; Tsutsumi, H.; Matsuda, Y.; Kawaguchi, M. Layered-structure BC_2N as a negative electrode matrix for rechargeable lithium batteries. *J. Electrochem. Soc.* **1992**, *139*, 1227–1230.
14. Shaijumon, M. M.; Ou, F. S.; Ci, L.; Ajayan, P. M. Synthesis of hybrid nanowire arrays and their application as high power supercapacitor electrodes. *Chem. Commun.* **2008**, 2373–2375.
15. Reddy, A. L. M.; Ramaprabhu, S. Nanocrystalline metal oxides dispersed multiwalled carbon nanotubes as supercapacitor electrodes. *J. Phys. Chem. C* **2007**, *111*, 7727–7734.
16. Park, J. H.; Ko, J. M.; Park, O. O. Carbon nanotube/RuO_2 nanocomposite electrodes for supercapacitors. *J. Electrochem. Soc.* **2003**, *150*, A864–A867.
17. Leela Mohana Reddy, A.; Ramaprabhu, S. Pt/SWNT-Pt/C nanocomposite electrocatalysts for proton-exchange membrane fuel cells. *J. Phys. Chem. C* **2007**, *111*, 16138–16146.
18. Shaijumon, M. M.; Ramaprabhu, S.; Rajalakshmi, N. Platinum/multiwalled carbon nanotubes-platinum/carbon composites as electrocatalysts for oxygen reduction reaction in proton exchange membrane fuel cell. *Appl. Phys. Lett.* **2006**, *88*, 253105.
19. Rajalakshmi, N.; Ryu, H.; Shaijumon, M.; Ramaprabhu, S. Performance of polymer electrolyte membrane fuel cells with carbon nanotubes as oxygen reduction catalyst support material. *J. Power Sources* **2005**, *140*, 250–257.
20. Reddy, A. L. M.; Shaijumon, M. M.; Gowda, S. R.; Ajayan, P. M. Coaxial MnO_2/carbon nanotube array electrodes for high-performance lithium batteries. *Nano Lett.* **2009**, *9*, 1002–1006.

21. Geim, A. K.; Novoselov, K. S. The rise of graphene. *Nat. Mater.* **2007**, *6*, 183–191.
22. Wang, D.; Choi, D.; Li, J.; Yang, Z.; Nie, Z.; Kou, R.; Hu, D.; Wang, C.; Saraf, L. V.; Zhang, J.; Aksay, I. A.; et al. Self-assembled TiO_2-graphene hybrid nanostructures for enhanced Li-ion insertion. *ACS Nano* **2009**, *3*, 907–914.
23. Wang, C.; Li, D.; Too, C. O.; Wallace, G. G. Electrochemical properties of graphene paper electrodes used in lithium batteries. *Chem. Mater.* **2009**, *21*, 2604–2606.
24. Paek, S.; Yoo, E.; Honma, I. Enhanced cyclic performance and lithium storage capacity of SnO_2/graphene nanoporous electrodes with three-dimensionally delaminated flexible structure. *Nano Lett.* **2009**, *9*, 72–75.
25. Li, X.; Cai, W.; An, J.; Kim, S.; Nah, J.; Yang, D.; Piner, R.; Velamakanni, A.; Jung, I.; Tutuc, E.; et al. Large-area synthesis of high-quality and uniform graphene films on copper foils. *Science* **2009**, *324*, 1312–1314.
26. Wang, X.; Li, X.; Zhang, L.; Yoon, Y.; Weber, P. K.; Wang, H.; Guo, J.; Dai, H. N-Doping of graphene through electrothermal reactions with ammonia. *Science* **2009**, *324*, 768–771.
27. Wei, D.; Liu, Y.; Wang, Y.; Zhang, H.; Huang, L.; Yu, G. Synthesis of N-doped graphene by chemical vapor deposition and its electrical properties. *Nano Lett.* **2009**, *9*, 1752–1758.
28. Panchakarla, L. S.; Subrahmanyam, K. S.; Saha, S. K.; Govindaraj, A.; Krishnamurthy, H. R.; Waghmare, U. V.; Rao, C. N. R. Synthesis, structure, and properties of boron- and nitrogen-doped graphene. *Adv. Mater.* **2009**, 4726–4730.
29. Ci, L.; Song, L.; Jin, C.; Jariwala, D.; Wu, D.; Li, Y.; Srivastava, A.; Wang, Z. F.; Storr, K.; Balicas, L.; et al. Atomic layers of hybridized boron nitride and graphene domains. *Nat. Mater.* **2010**, *9*, 430–435.
30. Shirley, D. A. High-resolution X-ray photoemission spectrum of the valence bands of gold. *Phys. Rev. B* **1972**, *5*, 4709.
31. Aurbach, D.; Ein-Eli, Y. The study of Li-graphite intercalation processes in several electrolyte systems using *in situ* X-ray diffraction. *J. Electrochem. Soc.* **1995**, *142*, 1746–1752.
32. Frackowiak, E.; Gautier, S.; Gaucher, H.; Bonnamy, S.; Beguin, F. Electrochemical storage of lithium in multiwalled carbon nanotubes. *Carbon* **1999**, *37*, 61–69.
33. Dahn, J. R.; Zheng, T.; Liu, Y.; Xue, J. S. Mechanisms for lithium insertion in carbonaceous materials. *Science* **1995**, *270*, 590–593.
34. Li, Y. F.; Zhou, Z.; Wang, L. B. CN_x nanotubes with pyridinelike structures: p-type semiconductors and Li storage materials. *J. Chem. Phys.* **2008**, *129*, 104703.
35. Li, C.; Sun, Q.; Jiang, G.; Fu, Z.; Wang, B. Electrochemistry and morphology evolution of carbon micro-net films for rechargeable lithium ion batteries. *J. Phys. Chem. C* **2008**, *112*, 13782–13788.